Applied Thermal Engineering 73 (2014) 380–390

Contents lists available at ScienceDirect

Applied Thermal Engineering

journal homepage: www.elsevier.com/locate/apthermeng

CFD simulation of heat transfer enhancement of Al_2O_3/water and Al_2O_3/ethylene glycol nanofluids in a car radiator

Vahid Delavari, Seyed Hassan Hashemabadi*

Computational Fluid Dynamics (CFD) Research Laboratory, School of Chemical Engineering, Iran University of Science and Technology, Narmak, Tehran 16846, Iran

HIGHLIGHTS

- CFD simulation of turbulent and laminar flow heat transfer of nanofluids in flat tube.
- Single and two-phase approaches were evaluated by comparing with experimental data.
- Despite the time consuming, two-phase approach has better prediction for nanofluids Nusselt number.

ARTICLE INFO

Article history:
Received 23 March 2014
Accepted 23 July 2014
Available online 1 August 2014

Keywords:
Nanofluid
Computational fluid dynamics
Heat transfer
Flat tube
Two-phase approach
Car radiator

ABSTRACT

The present numerical study simulated turbulent and laminar flow heat transfer in nanofluids (Al_2O_3 particles in water and ethylene glycol-based fluid) passing through a flat tube in 3D using computational fluid dynamics (CFD) for single and two-phase approaches. The advantages over pure base fluids were evaluated. Empirical correlations were used to calculate nanofluid viscosity and thermal conductivity as a function of the volumetric concentration of the nanoparticles. First, the Nusselt numbers of the pure water and pure ethylene glycol in flat tubes were compared with the experimental data. Next, the Nusselt numbers for both approaches were compared with those for experimental data at the same Reynolds number for different concentrations of nanoparticles. A small difference in the friction factors of the tube was observed between the two approaches and the Nusselt number for the two-phase model was markedly different from that for the single-phase model; however, the volumetric flow for the same heat transfer rate decreased and less pumping power was required for the nanofluids.

1. Introduction

In recent years, extensive research has been focused on nanofluids (metal or metal oxide particles typically less than 100 nm in size suspended in a base fluid) and their role in heat transfer. One important application for nanofluids is as a vehicle engine coolant. The very high surface area of nanoparticles, even at low concentrations, increases thermal conductivity. The significant increase in the thermal properties of nanofluids has attracted scientific attention in recent years. Choi [2] first used the term "nanofluid" for fluids with suspended nanoparticles; numerous studies in various fields have examined these types of fluids.

Kim et al. [3] experimentally investigated the effect of convective heat transfer in nanofluids under laminar and turbulent flow regimes. They used a straight circular cross-section of a tube with constant wall heat flux for laminar and turbulent flow regimes. The effects of the thermo-physical properties on models for predicting convective heat transfer coefficients of nanofluids at low concentrations were studied by Duangthongsuk and Wongwises [4]. They found that, at low concentrations of nanoparticles in the base fluid, the validity and accuracy of the experimental convective heat transfer coefficient depends more on empirical calibration of the system than on the thermo-physical models of nanofluids.

Peyghambarzadeh et al. [5] tested the increase in heat transfer for nanofluids based on turbulent flow of water in a car radiator. Ferrouillat et al. [6] reported on heat transfer and hydraulics of nanofluids with SiO_2 nanoparticles in a horizontal tube under constant wall temperature conditions. Their experiments were done at 20, 50 and 70 °C and Reynolds numbers of 200–10,000. In this study, an increase in convective heat transfer of nanofluids over pure water was reported.

The use of nanofluids in a plate heat exchanger was studied numerically and experimentally by Pantzali et al. [7] using a laminar flow regime. The thermal performance of the nanofluid

* Corresponding author. Fax: +98 21 7724 0495.
E-mail address: hashemabadi@iust.ac.ir (S.H. Hashemabadi).

http://dx.doi.org/10.1016/j.applthermaleng.2014.07.061
1359-4311/

Nomenclature

A	cross sectional area of the tube (m^2)
C_p	specific heat capacity (J/kg K)
D_h	hydraulic diameter of the tube (m)
d_p	nanoparticles diameter (m)
f	friction factor
h	heat transfer coefficient (W/m^2 K)
k	thermal conductivity (W/m K)
l	length of the tube (m)
Nu	Nusselt number (hd_{hy}/k)
P	pressure, Pa
Pr	Prandtl number ($C_p\mu/k$)
P_t	tube periphery (m)
Re	Reynolds number ($\rho u d_{hy}/\mu$)
T	temperature (K)
V	average velocity (m/s)
V_B	Brownian velocity (m/s)
X_H	hydrodynamic entry length (m)
X_T	thermal entry length (m)
W	power (W)

Greek letters

ρ	density (kg/m^3)
δ	distance between the centers of the particles (m)
μ	viscosity (kg/m s)
φ	nanoparticle volume fraction (%)
Φ	shape factor
ψ	particle sphericity

Subscripts

ave	peripheral average
bf	base fluid
nf	nanofluid
p	nanoparticle
k	component

containing 4% CuO nanoparticles was compared with pure water. The results indicated that, at a given heat transfer rate, the volumetric flow rate for nanofluids was lower than for pure water, which had a lower drop in pressure. Heat transfer coefficients for water-based CuO nanofluids in a laminar flow in a flat tube has been studied by Naraki et al. [8] and Peyghambarzadeh et al. [9]. Their results showed that the overall heat transfer coefficient increased as the nanoparticle concentration increased.

Demir et al. [10] did a 2D numerical study of single-phase forced convective heat transfer for Al_2O_3 and TiO_2 nanofluids in a horizontal counter current double pipe heat exchanger. They reported that heat transfer increased with the presence of nanoparticles in the base fluid. Keshavarz et al. [11] assumed constant heat flux in the tube wall for laminar flow heat transfer of nanofluids modeled using CFD in a fully developed region inside tubes with circular cross-sections. The single-phase simulation used nanoparticles with average diameters of 45 and 150 nm at concentrations of 1%, 2% and 4%. The results showed differences of up to 10% with the experimental data; they found that heat transfer increased as the concentration of the nanoparticles increased.

In the two-phase approach, the base fluid and nanoparticles are considered in two separate phases at different speeds and temperatures and the internal conflict of the nanofluid phase is used to solve the governing equations. Kalteh et al. [12] simulated nanofluids for forced convection heat transfer at a constant temperature in a micro-channel using laminar flow. The Eulerian–Eulerian two-phase approach was considered to simulate the nanofluids in the micro-channel and the equations of conservation of mass, momentum, and energy were solved for both phases using the finite volume method. The relative velocity and temperature of both phases were investigated and it was found that the difference between two-phase velocity and temperature distribution was negligible and the nanofluid concentration distribution was assumed to be uniform. The two-phase simulation results showed more heat transfer than the single-phase homogeneous model; in other words, the Nusselt numbers of the two-phase model were 50%–80% greater than for the single-phase approach.

Akbari et al. [13] developed a CFD model for single-phase and two-phase (VOF, mixture, and Eulerian) approaches. The results of the two-phase approach were closer to the experimental data than the results of the single phase. It was shown that both single-phase and two-phase approaches predicted similar flow fields, but the predictions for the thermal fields differed.

Many researchers have simulated the laminar flow of nanofluids through tubes with circular cross-sections, but few studied nanofluids in a flat tube. One study [1] experimentally investigated the flow of nanofluids through flat tubes and can be used for comparison of numerical results. In this study, the thermal and hydraulic performance of nanofluids in flat-tube exchangers was investigated numerically.

2. Mathematical modeling

2.1. Topic geometry

Fig. 1 shows the simulated geometry of a car radiator, including the vertical flat tubes with flat fins to remove heat from fluid to the air. These types of heat exchangers perform well and efficiently because of their flat tube design. This type of tube has a lower

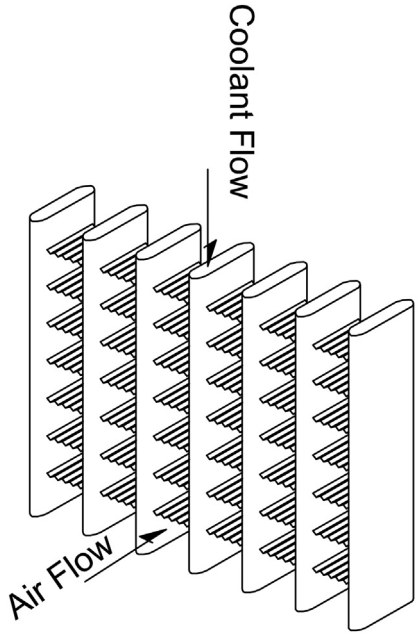

Fig. 1. Configuration of simulated air exchanger.

pressure drop on the air side than do circular cross-section tubes. The geometrical characteristics of the tube used in the air-cooled exchanger are shown in Fig. 2 [1].

2.2. The governing equations

The governing equations are assumed to be steady state for incompressible fluid and the fluid inside the tube has Newtonian behavior. The density of the water- and ethylene glycol-based nanofluids is almost constant under pressure. The Newtonian behavior of water-based Al_2O_3 nanofluids was reported by Das et al. [14] for nanoparticle concentrations of up to 4%. Ambient temperature and an air velocity through the air-cooled exchanger was assumed to constant. Inlet velocity and temperature of the flat tube was uniform. The gravity force was neglected because the viscous drag force (frictional force on tube walls) is much greater than the gravity force.

Thermal equilibrium was established between the nanoparticles and the base fluid. This assumption was used to calculate the specific heat capacity as reported by Xuan and Roetzel [19]. Particle deposition was neglected because the size and concentration of nanoparticles was very low and, with a good approximation, can be considered to be a homogeneous fluid. The high speed of the nanofluids through the flat tube does not allow settling of the nanoparticles. According to these conditions, the conservation equations are simplified as follows:

The continuity and momentum equations are respectively:

$$\nabla \cdot V = 0 \tag{1}$$

$$\rho_{nf}\left(\nabla \cdot V\right)V = -\nabla P + \left(\mu_{nf} + \mu^t\right)\nabla^2 V \tag{2}$$

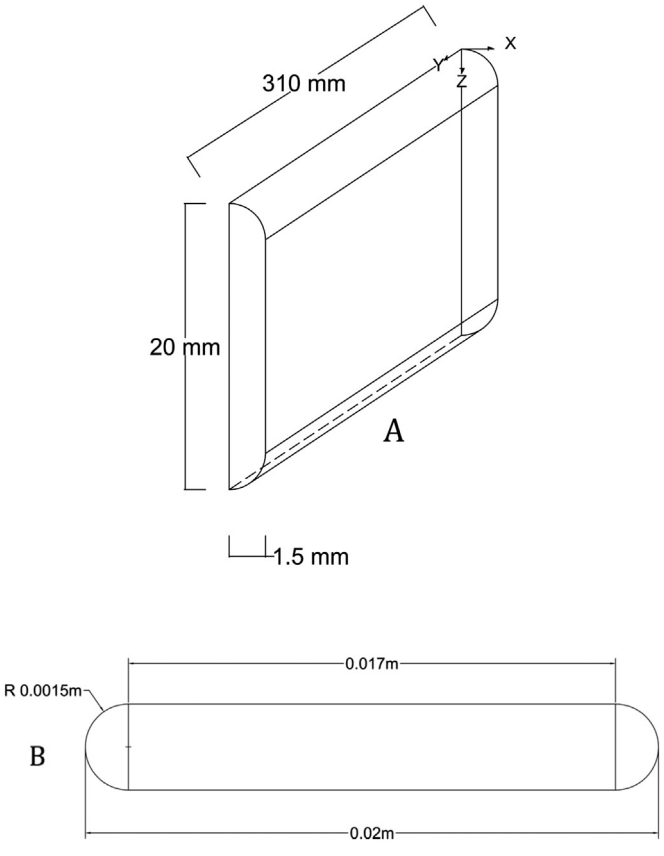

Fig. 2. Dimensions of flat tube used in this study [1] A) side view, B) top view.

The standard $k-\varepsilon$ model has been used for calculation of turbulence viscosity [27]:

$$\mu^t = C_\mu \frac{k^2}{\varepsilon} \tag{3}$$

The energy conservation equation is as bellow:

$$\rho_{nf} C_{pnf}\left(V \cdot \nabla\right)T = k_{nf}\nabla^2 T \tag{4}$$

2.3. The single phase model

More recent research suggests that, at a low volume concentration of nanoparticles in the base fluid, it can be assumed that the nanofluid will behave like a single-phase fluid [15]. This model considers the nanofluid as a homogeneous fluid which is strongly dependent to its physical properties. It is very important to use most proper correlations for the effective nanofluid properties to get correct results with solving the differential equations presenting conservation of mass, momentum and energy. Nanofluid properties rely on the volume fraction of particles as well as on the corresponding properties of the base fluid and the solid particles. Since the properties of the base fluid are temperature dependent, those of the nanofluid are also temperature dependent. Therefore, in this study all the nanofluid properties are described as function of the volume fraction and temperature [13].

The heat transfer coefficient and Nusselt number can be calculated respectively:

$$h_{nf}(\mathrm{CFD}) = \frac{C_{pnf}\rho_{nf}V_t A_t(T_{in} - T_{out})}{A_p(T_b - T_w)} \tag{5}$$

$$\mathrm{Nu}_{nf}(\mathrm{CFD}) = \frac{h_{nf}(\mathrm{CFD})D_h}{k_{nf}} \tag{6}$$

where T_b is the bulk temperature of the fluid, which is the average temperature of the inlet and outlet of flat tube. T_w is the flat tube wall surface temperature and A_t is cross section area of the flat tube (Fig. 2B).

2.4. The two-phase model

There are two general approaches to simulating solid–liquid flows. For a low volumetric concentration of solid particles, the best approach is the Lagrangian–Eulerian which assumes the Eulerian approach for the base fluid and Lagrangian approach for the particle phase. For high volumetric concentrations, the Eulerian–Eulerian approach is more suitable. The number of particles in the computational domain of a nanofluid is very high, even at low volumetric concentrations, because of the very small size of the nanoparticles. A nanofluid flow problem solved using the Lagrangian approach appears to be impossible because of the lack of adequate software, computer memory, and CPU. Therefore, due to less computational time, the mixture model based on Eulerian–Eulerian approach is considered for this study. The mass conservation equation for mixture models is as follows [13]

$$\nabla \cdot \left(\rho_{nf}\vec{v}_{nf}\right) = 0 \tag{7}$$

where

$$\vec{v}_{nf} = \frac{\sum_{k=1}^{2}\varphi_k\rho_k\vec{v}_k}{\rho_{nf}} \tag{8}$$

$$\rho_{nf} = \sum_{k=1}^{2} \varphi_k \rho_k \tag{9}$$

The momentum equation in steady state condition is:

$$\nabla \cdot \left(\rho_{nf} \vec{v}_{nf} \vec{v}_{nf}\right) = -\nabla p + \nabla \cdot \left[\mu_{nf}\left(\nabla \vec{v}_{nf}\right)\right] + \rho_{nf} \vec{g} + \nabla \cdot \left(\sum_{k=1}^{2} \varphi_k \rho_k \vec{v}_{dr,k} \vec{v}_{dr,k}\right) \tag{10}$$

$$\mu_{nf} = \sum_{k=1}^{2} \varphi_k \mu_k \tag{11}$$

Where drift velocity is defined as bellow:

$$\vec{v}_{dr,k} = \vec{v}_k - \vec{v}_{nf} \tag{12}$$

The energy conservation equation for mixture model is:

$$\nabla \cdot \sum_{k=1}^{2} (\varphi_k \vec{v}_k (\rho_k E_k + p)) = \nabla \cdot \left(k_{eff} \nabla T\right) + S_E \tag{13}$$

$$E_k = h_k - \frac{p}{\rho_k} + \frac{v_k^2}{2} \tag{14}$$

In this model, the solid particles are assumed to be a continuum, so its viscosity must be calculated. The lack of experimental data means that the solid viscosity for the solid–liquid two-phase mixture model is not available. The following method was used as an approximation for this study.

The pressure drop and average Nusselt number of a very dilute nanofluid with a nanoparticle volumetric concentration of 0.00001 (close to pure water or pure ethylene glycol) was compared with that of pure water at a Reynolds number of 9350 and that of pure ethylene glycol at a Reynolds number of 2440. Using trial and error, the viscosity of the nanoparticles changed up to the point at which the pressure drop and Nusselt number of the very dilute nanofluid, pure ethylene glycol, and pure water were equal. The viscosity of the nanoparticles in the water-based nanofluids was 0.00138 kg/m s and of the ethylene glycol-based nanofluids was 0.02 kg/m s. The difference between the pressure drop and average Nusselt number of the very diluted nanofluid with water was zero and of the ethylene glycol was 1.1%. This method has been validated by Kalteh et al. [12], who also showed that the viscosity of the solid phase is independent of the Reynolds number.

2.5. Thermo-physical properties of nanofluid

Usually Al_2O_3 nanofluid density and other nanofluids are measured by the digital density meter. However, the equation given by Pak and Cho [18] has a good agreement with the measured results. Thus, the density correlation used in this study is:

$$\rho_{nf} = \varphi \rho_p + (1 - \varphi)\rho_{bf} \tag{15}$$

where φ is the volumetric concentration of the nanoparticles.

Specific heat of nanofluids was obtained from the proposed correlation by Xuan and Roetzel [19]. Their equation is as follows:

$$C_{pnf} = \frac{\varphi \rho_p C_{pp} + (1 - \varphi)\rho_{bf} C_{pbf}}{\rho_{nf}} \tag{16}$$

Hamilton [20] has presented known model for conductive heat transfer coefficient.

$$k_{nf} = \frac{k_p + (\Phi - 1)k_{bf} - \varphi(\Phi - 1)\left(k_{bf} - k_p\right)}{k_p + (\Phi - 1)k_{bf} + \varphi\left(k_{bf} - k_p\right)} k_{bf} \tag{17}$$

where Φ is an empirical shape factor and is equal to $\Phi = 3/\Psi$. Particle sphericity (Ψ) is the ratio of the surface area of a sphere that has same volume as the particle over the particle surface area. In this study, Φ was considered equal to 3 [1].

Recently Masoumi et al. [21] presented an analytical model to calculate the nanofluid viscosity of the fluid with respect to Brownian motion of nanoparticles:

$$\mu_{nf} = \mu_{bf} + \frac{\rho_p V_B d_p^2}{72 C \delta} \tag{18}$$

where V_B is the velocity of Brownian motion and is defined as follows:

$$V_B = \frac{1}{d_p} \sqrt[3]{\frac{18 K_b T}{\pi \rho_p d_p}} \tag{19}$$

and K_b is Boltzmann's constant and is equal to 1.38×10^{-23}. As can be seen, Brownian velocity is a function of temperature. In Eq. (18) ρ_p and d_p are respectively the density and diameter of the nanoparticles and δ represents the distance between the centers of two particles which is:

$$\delta = \sqrt[3]{\frac{\pi}{6\varphi}} d_p \tag{20}$$

In Eq. (18) C is a correction factor and it is calculated as follows:

$$C = \frac{a\varphi + b}{\mu_{bf}} \tag{21}$$

where a and b are empirical coefficients, according to the Kole and Dey [22] for the nanofluid discussed in this study are respectively -0.00004 and 7.13×10^{-7}. According to the new report of Masoumi et al. [21] because the Reynolds number for the nanoparticles is much lower than one, creeping flow around the nanoparticles can be solved with a correction factor. They defined factor N as follows:

$$N = a\varphi + b \tag{22}$$

where a and b are the empirical coefficients in Eq. (21). Relative viscosity is defined as:

$$\frac{\mu_{nf}}{\mu_{bf}} = 1 + \frac{\rho_p V_B d_p^2}{72 N \delta} \tag{23}$$

As seen, the relative viscosity is independent of the base fluid viscosity and depends on the temperature, diameter, density, and volumetric concentration of the nanoparticles in the base fluid. The density and diameter of the nanoparticles were considered constant and equal to 4000 kg/m^3 [22], and 20 nm [1], respectively.

2.6. Boundary conditions and CFD simulation

Numerical calculations were performed in a laminar flow regime for nanofluids based on ethylene glycol and in turbulent flow for nanofluids based on water from a volumetric concentration of zero to 1% for alumina (Al_2O_3) nanoparticles. Table 1 shows the range of operating conditions in this study. The symmetry of the flat tube decreased the computation time and increased the computing

Table 1
The range of operating conditions in this study.

Parameter	Water-based nanofluids	Ethylene glycol-based nanofluids
Types of nanoparticles	γ-Al_2O_3	γ-Al_2O_3
Nanoparticle volumetric concentration	Up to 1%	Up to 1%
Reynolds number	9000–23,000	1200–2500
Flow regime	Turbulent	Laminar
Flat tube inlet temperature (°C)	35–50	45–60

speed; half of a flat tube of an air cooled exchanger was considered to be the computational domain.

Fig. 4 illustrates the QUADMAP scheme used to mesh the computational domain. The boundary conditions in Fig. 3 were used for the velocity inlet, pressure outlet, wall and symmetry. Cell density near the wall was considered to be higher to properly display fluid bulk heat transfer near the wall. A square grid was chosen because it shows greater density around the wall. Since the turbulent flow of pure water and water-based nanofluids are at a Reynolds number of less than 106, an enhanced wall treatment with pressure gradient and thermal effects can be used for the simulations.

The nanofluid was subjected to following boundary conditions (Fig. 3):

- Velocity inlet, because inlet temperature and velocity are known. The turbulence intensity was 10% and the hydraulic diameter of flat tube under consideration was 5.3×10^{-3} mm.
- Pressure outlet, because nanofluid flow inside the flat tube was not developed through the tube length.
- Wall of the computational domain was assumed with convection boundary condition with heat transfer coefficient of 150 W/m^2 K [16,17] and the air temperature of 303 K [1].

The set of governing equations was resolved by the finite volume method [23,28] on a computer with 2.5 GHz dual core and 4 GB RAM. The first-order upwind method was used to discretize

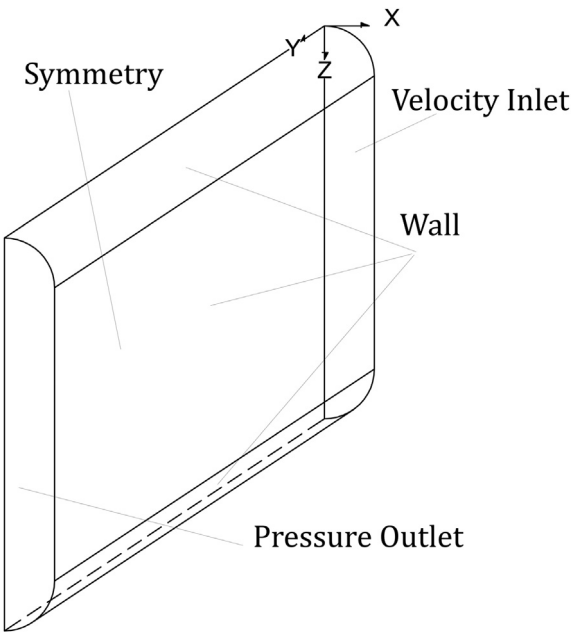

Fig. 3. Boundary conditions for the computational domain.

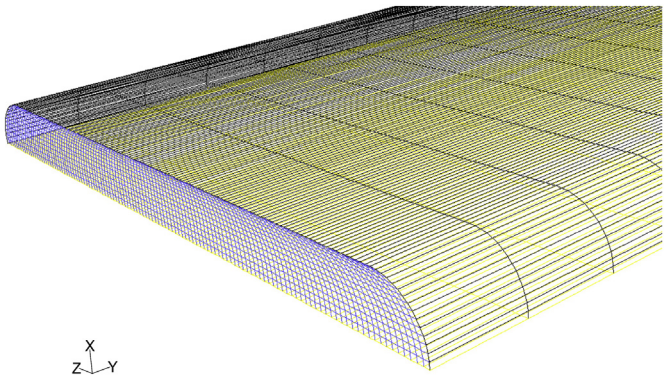

Fig. 4. Layout of mesh #2 which is used in this study.

the convection terms from the conservation equations. The staggered grid was implemented for simulations where velocity components were calculated on the control volume faces and the flow variables were obtained in the central node of the control volume. The linear algebraic system obtained from discretization was solved using the Gauss–Seidel method. For all simulations performed in this study, a converged solution in an iterative process for the residuals of the continuity, momentum and energy conservation equations was considered to be less than 10^{-6}, and 10^{-9}, respectively.

3. Results and discussion

3.1. Mesh independency of results

To verify mesh independence and achieve the minimum number of cells for accurate computational results, five mesh sizes were selected for discretization in the computational domain (Table 2). Mesh #5 was tested to decrease the computational cell length in the *Y* direction; the mesh size in this direction is similar to the cell size in two other directions. The cell size for mesh #2 (Fig. 4) in the *Y* direction is 15.5 times the cell size in the *Z* direction, which this ratio for mesh #5 is equal to 5.

Table 2 shows the maximum velocity and temperature for laminar flow of pure water through a flat tube at a Reynolds number of 200 for different meshes. The velocity and temperature profiles for mesh #1 do not match those of the other mesh sizes. Values for meshes #2–#5 overlap and it can be concluded that mesh independence is reached using mesh #2 and finer meshes. Accordingly, all simulations used mesh #2. First order upwind method, is easiest and most economical for discretization of convection terms in governing equations. The validity of first order upwind method was reviewed using two computational runs. The results of both methods using mesh #2 are shown in Table 3 briefly. The maximum difference between the two methods is less than 0.021 percent. The number of iterations for the second-order

Table 2
Mesh independence study in the fully developed region of heat and fluid flow ($Y = 0.25$ m, $Z = 0.01$ m) for pure water at Reynolds 200.

Series	Mesh, (x, y, z)	Maximum speed, m/s	The maximum temperature, K	Computational time, min
1	$80 \times 60 \times 10$	0.040545	311.584	41
2	$120 \times 120 \times 15$	0.040693	311.596	440
3	$130 \times 130 \times 20$	0.040736	311.599	1167
4	$140 \times 140 \times 20$	0.040716	311.602	1291
5	$120 \times 372 \times 15$	0.040724	311.601	1353

Table 3
Comparison of the first and second order upwind scheme.

Axial location, m	Parameter	First order	Second order	Percent difference
$Y = 0.15$	Temperature, K	312.266	312.275	0.002882
$Y = 0.250$	Temperature, K	311.596	311.604	0.002567
$Z = 0.000463$	Velocity, m/s	0.036804	0.036811	0.020646
$Z = 0.001213$	Velocity, m/s	0.0140478	0.0140506	0.019928

method increased 20% and computational time increased by 1.5 times without creating an appreciable difference in the results.

3.2. Validation of computational procedures

Two-phase (nanoparticle concentration was assumed to be zero) and single-phase simulations were done for pure water in turbulent flow at 50 °C and pure ethylene glycol in laminar flow at 40 °C. The Reynolds numbers were then compared with the empirical data reported by Peyghambarzadeh et al. [1].

The numerical results for pure water have been compared with Dittus and Boelter [24] and Gnielinski [25] empirical correlations which have following form respectively.

$$\mathrm{Nu} = 0.0236\mathrm{Re}^{0.8}\mathrm{Pr}^{0.3} \tag{24}$$

$$\mathrm{Nu} = \frac{\left(\frac{f}{8}\right)(\mathrm{Re}-1000)\mathrm{Pr}}{1+12.7\left(\frac{f}{8}\right)^{0.5}\left(\mathrm{Pr}^{\frac{2}{3}}-1\right)} \tag{25}$$

where f, is the coefficient of friction which is defined as follows:

$$f = (0.79\ln\mathrm{Re} - 1.69)^{-2} \tag{26}$$

Fig. 5 shows good agreement between the CFD simulation for the single-phase and two-phase approaches with the correlations from Dittus and Boelter [24] and Gnielinski [25]. The absolute average error between the CFD results and Dittus and Boelter correlation is 4.54%; in Gnielinski, this value is 10.5%. The numerical results of the two-phase models (zero nanoparticles concentration) and pure water and pure ethylene glycol fully coincide.

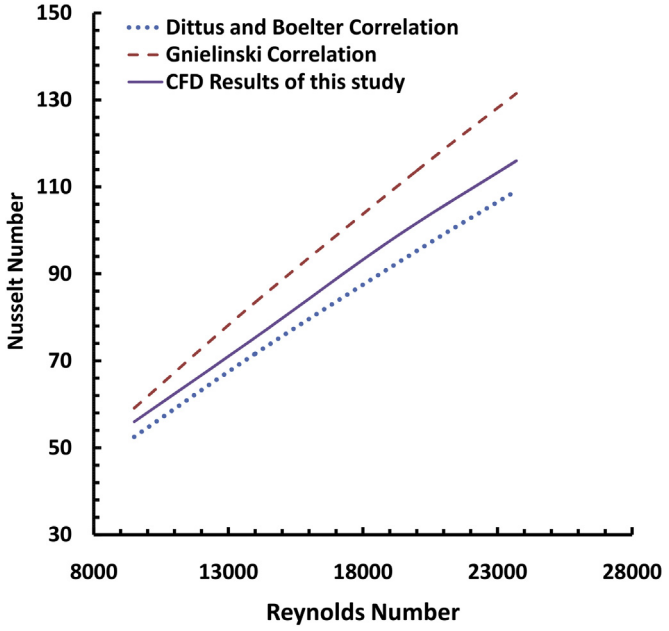

Fig. 5. Comparison of the numerical results of pure water (inlet temperature 50°°C) with existing correlations.

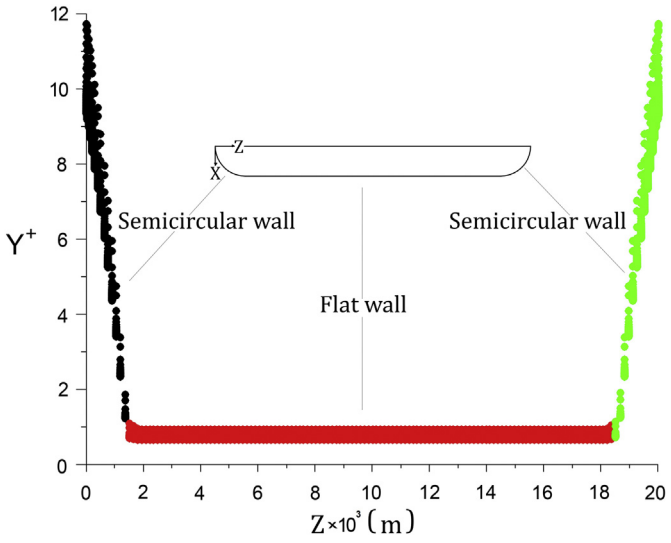

Fig. 6. Y^+ test for pure water at inlet temperature of 50°°C and Reynolds 9500.

Fig. 6 shows Y^+ at the flat tube wall for a Reynolds of 9500 with pure water flowing through the tube. Enhanced wall treatment was implemented in the turbulent flow simulation, which should produce a Y^+ value equal to one; the figure indicates that this holds true for most parts of the flat tube wall.

The numerical results for pure ethylene glycol were compared with the experimental data from Peyghambarzadeh et al. [1] and Vajjha et al. [26] correlations in Eq. (27).

$$\begin{cases} \mathrm{Nu} = 1.9421\left(\mathrm{RePr}\frac{D_h}{z}\right)^{0.3} & \left(\mathrm{RePr}\frac{D_h}{z}\right) \geq 33.33 \\ \mathrm{Nu} = 6.1 + 0.003675\left(\mathrm{RePr}\frac{D_h}{z}\right) & \left(\mathrm{RePr}\frac{D_h}{z}\right) \leq 33.33 \end{cases} \tag{27}$$

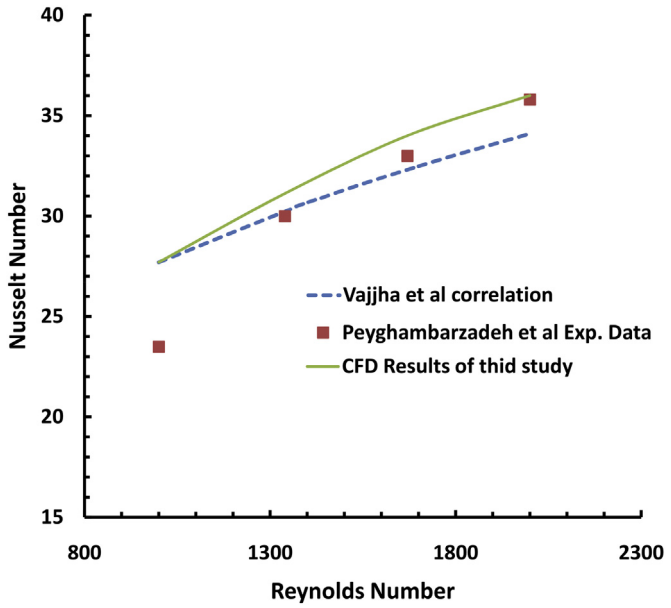

Fig. 7. Comparison of the numerical results for pure ethylene glycol (inlet temperature 40 °C) with experimental data [1] and existing correlations (Eq. (29)).

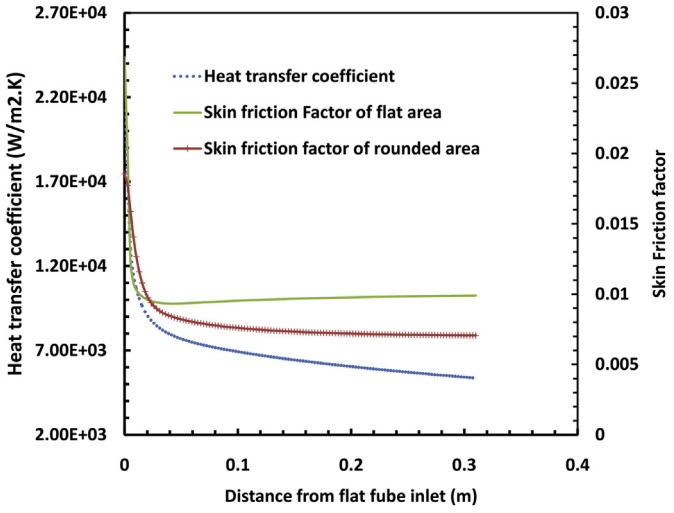

Fig. 8. Variation of heat transfer coefficient and the local friction coefficient along the tube wall for the pure water in Reynolds number of 9500 and inlet temperature of 50 °C.

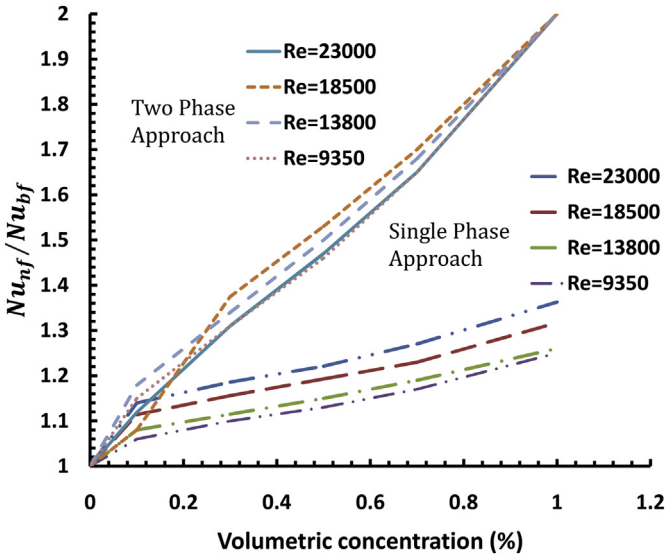

Fig. 9. Variations of the numerical results of Nu_{nf}/Nu_{bf} for water based nanofluids with different volumetric concentration of nanoparticles for inlet temperature of 45 °C and the same Reynolds numbers.

Fig. 7 confirms that the numerical results provide a good approximation. The mean absolute average error between the CFD results for both single-phase and two-phase approaches with experimental data is 5.56%; this value for the empirical correlation is 2.8%.

3.3. Local heat transfer coefficient and friction factor

Fig. 8 shows local heat transfer and local skin friction factor along the length of the wall in the flat tube. The results for pure water are an inlet temperature of 50 °C and a Reynolds number of 9500. Since the thermal and hydrodynamic boundary layer thicknesses are zero at the entrance to the tube, the convection coefficient and wall skin friction factor are very large at $Y = 0$. As both boundary layers develop, the locally-averaged convective heat transfer coefficient (h) and the locally averaged skin friction factor decrease rapidly.

3.4. Effect of nanoparticles concentration on Nusselt number

According to experimental data [1], nanofluids with different concentrations of 0.1, 0.3, 0.5, 0.7 and 1 volume percent of Al_2O_3 nanoparticles in water or ethylene glycol base fluid have been examined with different Reynolds numbers inside the flat tube. Also, the experiments were carried out at different input temperatures of 35, 40, 45, 50 and 60 °C to show the effect of temperature on the heat transfer coefficient.

Table 4 shows the results of the numerical calculations for the single-phase and two-phase approaches at the same Reynolds numbers. Fig. 9 shows the ratio of the Nusselt number for the nanofluid to that for water-based fluid at different Reynolds numbers and volumetric nanoparticle concentrations at an inlet temperature of 45 °C. As shown, the Nusselt number increased uniformly as the Reynolds number and concentration of nanoparticles increased. Kalteh et al. [12] found that the numerical results of the two-phase approach were 10%–32% greater than for the single-phase approach.

Table 5 shows the results of numerical calculations for single-phase and two-phase ethylene glycol-based nanofluids. The table shows a regular increase in the Nusselt numbers as the ethylene glycol-based nanofluid Reynolds numbers increase. It is clear that slight increases in nanoparticles in the cooling base fluid changed the thermo-physical properties of the fluid, increasing density, thermal conductivity, and viscosity and slightly decreasing the specific heat; this resulted in a significant increase in heat transfer by the nanofluid. The Brownian motion of the nanoparticles inside the fluid is a very important factor in increasing heat transfer by the nanofluid. The random motion of the nanoparticles in the fluid

Table 4
Numerical results of Nusselt number for two approaches for different volumetric concentration of nanofluids based on water with inlet temperature of 45 °C.

	Reynolds number	0%[a]	0.1%	0.3%	0.5%	0.7%	1%
		Nu					
Single-phase approach	23,000	118	135	140	144	150	161
	18,500	96	107	111	114	118	126
	13,800	78	84	87	90	93	99
	9350	58	62	64	66	68	73
Two-phase approach	23,000	118	132	155	174	195	239
	18,500	96	104	132	147	164	199
	13,800	78	92	105	117	131	159
	9350	58	67	76	85	96	117

[a] Pure water.

Table 5
Results of two approaches numerical simulation of Nusselt number for nanofluids with different volumetric concentrations based on ethylene glycol for inlet temperature of 45 °C.

	Reynolds number	0%[a]	0.1%	0.3%	0.5%	0.7%	1%
		Nu					
Single phase approach	2440	37	39.6	40.8	41.8	43.1	45.6
	2030	35	36.7	37.8	38.8	39.9	42.3
	1630	32	33.5	34.5	35.5	36.5	38.7
	1220	28	29.8	30.7	31.6	32.5	34.5
Two phase approach	2440	37	44.3	53.9	63.26	72.6	88
	2030	35	40.9	49.9	58.5	67.1	81.3
	1630	32	37.4	45.6	53.39	61.2	74
	1220	28	33.2	40.5	47.4	54.2	65.6

[a] Pure ethylene glycol.

decreased the boundary layer thickness, increasing heat transfer between the wall and the bulk fluid [9].

The numerical results of the two-phase approach were 10%–45% greater than for the single-phase approach. The experimental data [1] and previous studies [12,13] confirm that the two-phase model better predicts the Nusselt number of the experimental data.

3.5. Effect of nanoparticle concentration on friction factor

Fig. 10A and B shows changes in the local surface friction coefficient along the length of the flat tube length at different concentrations of Al_2O_3 nanoparticles and the same input velocity. The figures indicate that the local surface friction coefficient increased as the concentration of nanoparticles increased. This will increase the flow pressure drop in the flat tube.

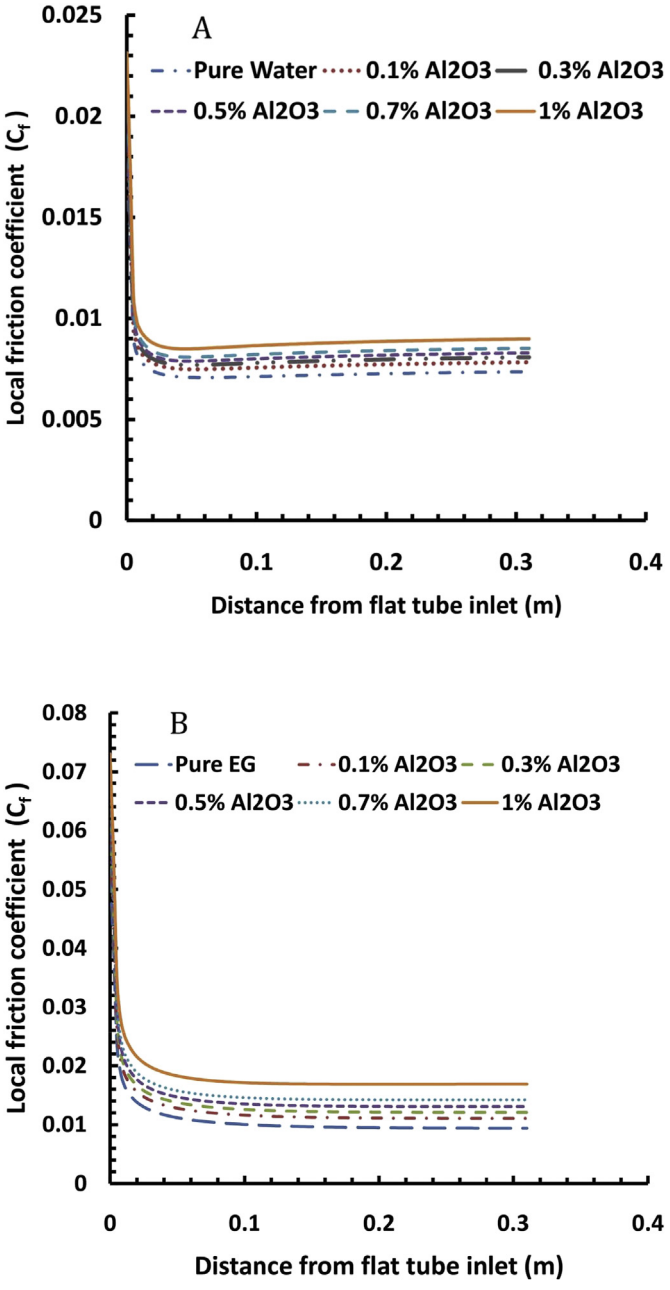

Fig. 10. Changes in local friction coefficient along the flat tube for different concentrations of Al_2O_3 nanoparticles in A) water based nanofluids, B) ethylene glycol based nanofluids with the same input velocity of 2.61245 m/s and 3.35338 m/s respectively and inlet temperature of 45 °C.

The computations were carried out for a uniform input velocity of 2.61245 m/s, equivalent to Reynolds number of 12,866 for 1% nanofluid and 23,000 for water base fluid due to its lower viscosity, and a uniform input velocity of 3.35338 m/s, equivalent to Reynolds number of 1360 for 1% nanofluids and 2440 for ethylene glycol base fluid, because its viscosity is lower. The surface friction coefficient for 1% nanofluid is 1.2 times that of the water based fluid and 1.8 times that of the ethylene glycol based fluid.

3.6. Effect of inlet temperature on Nusselt number

Fig. 11 shows Nusselt numbers of water-based nanofluid at different inlet temperatures. In this figure, the numerical results of single-phase and two-phase approaches are compared. It is clear that increasing the temperature at the flat tube inlet increased heat transfer slightly. An increase in inlet temperature from 35 to 50 °C for the water-based 1% nanofluid increased the Nusselt number for the single-phase approach by 4% and for the two-phase approach by 5%.

Fig. 12 shows the Nusselt numbers for ethylene glycol-based nanofluid at different inlet temperatures and the single-phase and two-phase numerical results were compared with the experimental data [1]. For 0.7% ethylene glycol-based nanofluid, increases in inlet temperature from 45 to 60 °C increased the experimental Nusselt numbers by 6%; the single-phase numerical results increased 0.5% and the two-phase numerical results increased 2% over that of pure ethylene glycol-based fluid. As seen, the results of the two-phase approach were closer to the experimental data than the results of the single-phase approach. The reasons for these differences are:

1. The wall thickness of the flat tube was set to zero in the simulation, neglecting heat dissipation by thermal conductivity in a solid wall. This created less heat transfer resistance for the numerical model over the experimental model.
2. The tube cross-section area of the flat tube was calculated based on the results of Peyghambarzadeh et al. [1]. The differences between the calculated cross-section and that of experimental case created differences in the hydraulic diameter and heat transfer surface of the flat tube.
3. The air velocity was assumed to be constant and uniform around the flat tube, which is not true in the actual case; thus, velocity

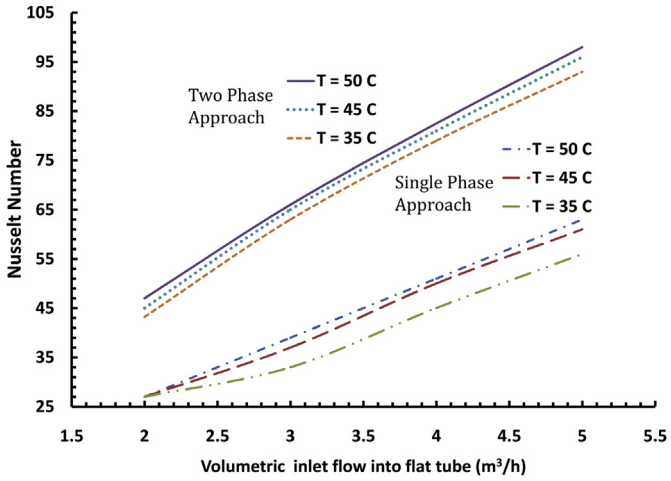

Fig. 11. Variation of Nusselt numbers of 1% Al_2O_3/water nanofluid for different inlet temperatures.

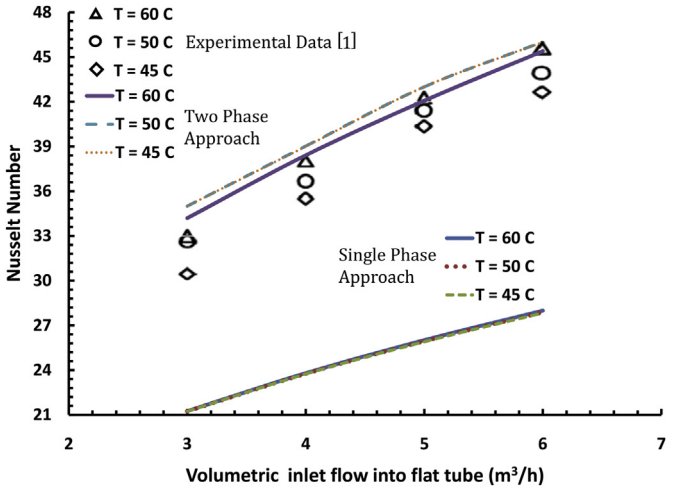

Fig. 12. Comparison of 0.7% Al_2O_3/ethylene glycol nanofluid Nusselt numbers with experimental data [1] for different inlet temperatures.

distribution around the impeller is different than in the central area.

4. The inlet velocity for the flat tube was assumed to be uniform and constant, but the numerical and empirical calculations based on this assumption could be in error. In the actual case, the head of a car radiator distributes inlet fluid non-uniformly through the tubes.

3.7. Effect of Reynolds number on average Nusselt number

Fig. 13 shows the average heat transfer coefficient and the average Nusselt number along the flat tube for water-based nanofluids that are defined as follows:

$$\overline{h} = \frac{1}{L}\int_0^L h_{ave} dY \tag{28}$$

$$\overline{Nu} = \frac{1}{L}\int_0^L Nu_{ave} dY \tag{29}$$

In general, the average heat transfer coefficient and Nusselt number increase with increasing the Reynolds number. Increasing

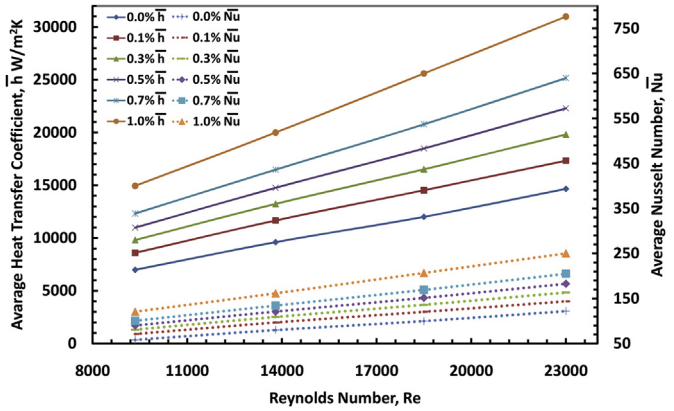

Fig. 13. The average heat transfer coefficient and average Nusselt numbers for 1% Al_2O_3/water nanofluid.

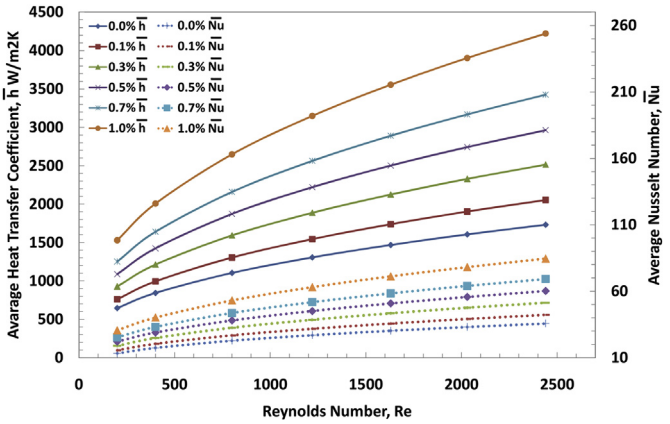

Fig. 14. The average heat transfer coefficient and average Nusselt numbers for 1% Al_2O_3/ethylene glycol nanofluid.

in the concentration of nanoparticles in a constant Reynolds number enhances the average Nusselt number. For a Reynolds number of 23,000, a 1% nanofluid produced an average Nusselt number that was 205% higher than for pure water. Fig. 14 shows the average heat transfer coefficients and average Nusselt numbers for

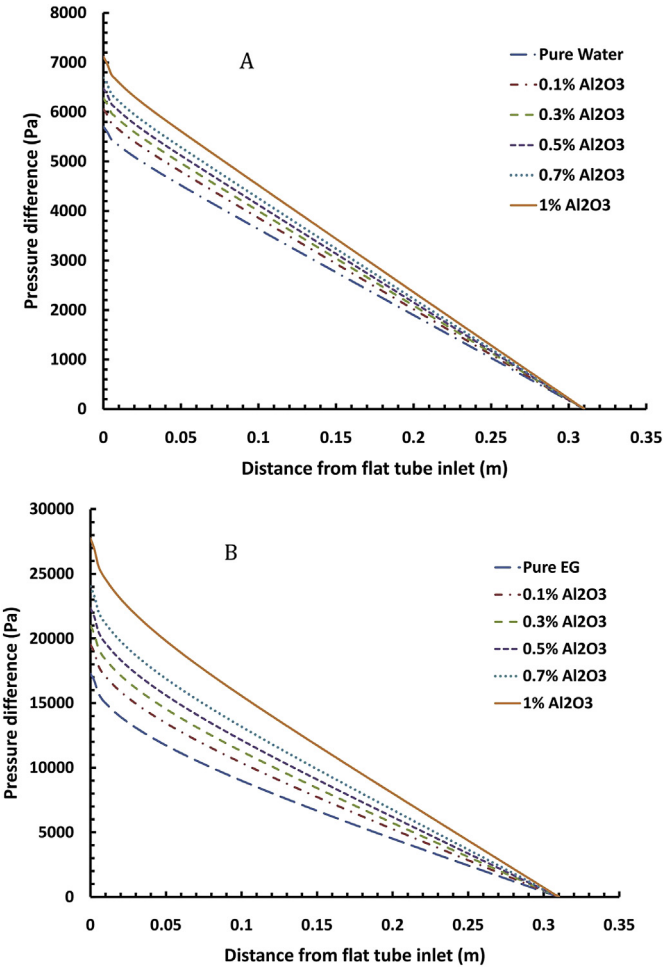

Fig. 15. Pressure drop inside the tube flat for nanofluids based on A) water B) ethylene glycol at Reynolds number of 23,000 and 2440 respectively and inlet temperature of 45 °C.

Table 6
Comparison of various parameters for different concentrations of the Al_2O_3 nanofluid with water base fluid for a constant heat transfer.

Type of nanofluid	Al_2O_3/water					
Concentration (%)	0	0.1	0.3	0.5	0.7	1
h (W/m^2 K)	14,660	14,660	14,660	14,660	14,660	14,660
Reynolds number, Re	23,000	18,500	15,800	13,800	11,900	9200
Density (kg/m^3)	990.2	993.2	999.2	1005.25	1011.3	1020.3
Viscosity (kg/m s)	5.96×10^{-4}	7.04×10^{-4}	7.73×10^{-4}	8.39×10^{-4}	9.18×10^{-4}	1.10×10^{-3}
Velocity (m/s)	2.6125	2.4742	2.3075	2.1734	2.0386	1.8680
Skin friction, $\overline{C_f}$	0.00702	0.00715	0.0073	0.00745	0.00763	0.0078
Pressure loss (Pa)	5549.73	5085.36	4543.15	4138.39	3751.26	3248.72
Power (W)	28.6254	24.8419	20.6976	17.7585	15.0986	11.9820
% Power reduction	–	13.217	27.695	37.962	47.254	58.142

Table 7
Comparison of various parameters for different concentrations of the Al_2O_3 nanofluid with the ethylene glycol base fluid for a constant heat transfer.

Type of nanofluid	Al_2O_3/ethylene glycol					
Concentration (%)	0	0.1	0.3	0.5	0.7	1
h (W/m^2 K)	1732	1732	1732	1732	1732	1732
Reynolds number, Re	2440	1620	980	660	460	280
Density (kg/m^3)	1098.3	1101.2	1107	1112	1118.61	1127.3
Viscosity (kg/m s)	0.008	0.00945	0.01038	0.01126	0.01232	0.01473
Velocity (m/s)	3.3534	2.6241	1.7338	1.2609	0.9559	0.6906
Skin friction, $\overline{C_f}$	0.01014	0.0125	0.0175	0.025	0.0312	0.045
Pressure loss (Pa)	14,653	11,088	6812	5171	3731	2830
Power (W)	97.0177	57.4498	23.3202	12.8735	7.0408	3.8589
% Power reduction	–	40.784	75.963	86.731	92.743	96.022

ethylene glycol-based nanofluids. The average Nusselt number increased as the Reynolds number increased. Increasing the nanoparticle concentration at a constant Reynolds number increased the average Nusselt number. For example, for a Reynolds number of 2440, the 1% nanofluid produced a Nusselt number that is 237% higher than that for pure ethylene glycol.

3.8. Effect of nanoparticle concentration on the pressure drop

The pressure drop in the flat tube for the water- and ethylene glycol-based nanofluids are shown in Fig. 15A and B at an inlet velocities of 2.61245 m/s (Reynolds 23,000) and 3.35338 m/s (Reynolds 2440), respectively, at an inlet temperature of 45 °C. As these figures show, the increase in the concentration of nanoparticles in the base fluid increased the pressure drop. Pantzali et al. [7] reported that, for a given heat transfer rate, the nanofluid volumetric flow rate was less than for the base fluid having a low pressure drop; in other words, less pumping power was required.

Figs. 13 and 14 can be used to demonstrate the effect of nanoparticle concentration on pumping power found by Vajjha et al. [26]; the Reynolds numbers for nanofluids at different concentrations with same convective heat transfer coefficients were lower than for pure base fluids (Tables 6 and 7). For example, Table 6 shows that pure water with a Reynolds number of 23,000 produces an average convective heat transfer coefficient of 14,660 W/m^2 K (Fig. 13). This value occurs for 1% nanofluid at a Reynolds number of 9200. Tables 6 and 7 show the velocities calculated from the Reynolds numbers and average tube friction factors from the numerical. So the pressure drop is calculated from the following formula for flat tube:

$$\Delta P = \overline{C_f} \frac{4L}{D_h} \frac{1}{2} \rho V^2 \tag{30}$$

where the average friction factor can be calculated as follows:

$$\overline{C_f} = \frac{1}{L} \int_0^L C_{f\ ave} dY \tag{31}$$

and the pumping power required to circulate the fluid is equal to:

$$W = AV(\Delta P) \times 34 \tag{32}$$

Tables 6 and 7 show that nanofluids require less pumping power at lower velocities than do the pure base fluids to exercise the same level of heat transfer. For constant heat transfer, the pumping power required for nanofluids decreased as the concentration of the nanoparticles increased.

4. Conclusion

The behavior of water- and ethylene glycol-based Al_2O_3 nanofluids were numerically studied in turbulent and laminar flow regimes in a flat tube. Both approaches were considered to evaluate the forced convection of the nanofluids through the 3D computational domain. New correlations from experimental data were used to calculate nanofluid viscosity and thermal conductivity as a function of nanoparticle volumetric concentration and temperature. The Nusselt numbers for both approaches at different nanoparticle concentrations and the same Reynolds number was compared with experimental and well-known correlations.

The numerical results were the same as for the experimental data, indicating that increasing the concentration of nanoparticles in the base fluid increased the heat transfer coefficient and the Nusselt number. The influence of inlet temperature on Nusselt number of a nanofluid at the same volumetric flow rate was compared with experimental data. It was shown that the two-phase model better predicted the Nusselt number for the experimental data than did the single-phase approach.

Tube friction factor results showed that the tube friction coefficient increased as the concentration of nanoparticles in the nanofluid increased. The results indicate that, for a given heat transfer rate, the required nanofluid volumetric flow rate was less than that for the pure base fluid flow having a low pressure drop, decreasing the pumping power required. Nanofluids are a promising solution for optimal design of a heat exchange system when the size of the equipment is critical.

References

[1] S.M. Peyghambarzadeh, S.H. Hashemabadi, S.M. Hoseini, M. Seifi, Experimental study of heat transfer enhancement using water/ethylene glycol based nanofluids as a new coolant for car radiators, Int. Commun. Heat Mass Transfer 38 (2011) 1283–1290.

[2] S.U.S. Choi, Enhancing thermal conductivity of fluids with nanoparticles, in: Proceedings of the ASME International Mechanical Engineering Congress and Exposition, vol. 231, ASME, San Francisco, CA, USA, 1995, pp. 99–105.

[3] D. Kim, Y. Kwon, Y. Cho, Convective heat transfer characteristics of nanofluids under laminar and turbulent flow conditions, Curr. Appl. Phys. 9 (2009) 119–123.

[4] W. Duangthongsuk, S. Wongwises, Effect of thermophysical properties models on the predicting of the convective heat transfer coefficient for low concentration nanofluid, Int. Commun. Heat Mass Transfer 35 (2008) 1320–1326.

[5] S.M. Peyghambarzadeh, S.H. Hashemabadi, M. Seifi Jamnani, S.M. Hoseini, Improving the cooling performance of automobile radiator with Al_2O_3/water nanofluid, Appl. Therm. Eng. 31 (2011) 1833–1838.

[6] S. Ferrouillat, A. Bontemps, J. Ribeiro, Gruss, O. Soriano, Hydraulic and heat transfer study of SiO_2/water nanofluids in horizontal tubes with imposed wall temperature boundary conditions, Int. J. Heat Fluid Flow 32 (2011) 424–439.

[7] M.N. Pantzali, A.G. Kanaris, K.D. Antoniadis, A.A. Mouza, S.V. Paras, Effect of nanofluids on the performance of a miniature plate heat exchanger with modulated surface, Int. J. Heat Fluid Flow 30 (2009) 691–699.

[8] M. Naraki, S.M. Peyghambarzadeh, S.H. Hashemabadi, Y. Vermahmoudi, Parametric study of overall heat transfer coefficient of CuO/water nanofluids in a car radiator, Int. J. Therm. Sci. 66 (2013) 82–90.

[9] S.M. Peyghambarzadeh, S.H. Hashemabadi, M. Naraki, Y. Vermahmoudi, Experimental study of overall heat transfer coefficient in the application of dilute nanofluids in the car radiator, Appl. Therm. Eng. 52 (2013) 8–16.

[10] H. Demir, A.S. Dalkilic, N.A. Kürekci, W. Duangthongsuk, S. Wongwises, Numerical investigation on the single phase forced convection heat transfer characteristics of TiO_2 nanofluids in a double-tube counter flow heat exchanger, Int. Commun. Heat Mass Transfer 38 (2011) 218–228.

[11] M. Keshavarz, M. Darabi, S.M. Hossein Haddad, R. Davarnejad, Modeling of convective heat transfer of a nanofluid in the developing region of tube flow with computational fluid dynamics, Int. Commun. Heat Mass Transfer 38 (2011) 1291–1295.

[12] M. Kalteh, A. Abbassi, M. Saffar-Avval, J. Harting, Eulerian–Eulerian two-phase numerical simulation of nanofluid laminar forced convection in a microchannel, Int. J. Heat Fluid Flow 32 (2011) 107–116.

[13] M. Akbari, N. Galanis, A. Behzadmehr, Comparative analysis of single and two-phase models for CFD studies of nanofluid heat transfer, Int. J. Therm. Sci. 50 (2011) 1343–1354.

[14] S.K. Das, N. Putra, W. Roetzel, Pool boiling characteristics of nano-fluids, Int. J. Heat Mass Transfer 46 (2003) 851–862.

[15] A. Akbarinia, A. Behzadmehr, Numerical study of laminar mixed convection of a nanofluid in horizontal curved tubes, Appl. Therm. Eng. 27 (2007) 1327–1337.

[16] K.W. Park, H.Y. Pak, Flow and heat transfer characteristics in flat tubes of a radiator, part A, Numer. Heat Transfer 41 (2002) 19–40.

[17] W.M. Kays, A.L. London, Compact Heat Exchangers, third ed., McGraw-Hill, New York, 1984, pp. 45–64.

[18] B.C. Pak, Y.I. Cho, Hydrodynamic and heat transfer study of dispersed fluids with submicron metallic oxide particles, Exp. Heat Transfer 11 (1998) 151–170.

[19] Y. Xuan, W. Roetzel, Conceptions of heat transfer correlation of nanofluids, Int. J. Heat Mass Transfer 43 (2000) 3701–3707.

[20] R.L. Hamilton, O.K. Crosser, Thermal conductivity of heterogeneous two-component systems, Ind. Eng. Chem. Fundam. 1 (3) (1962) 187–191.

[21] N. Masoumi, N. Sohrabi, A. Behzadmehr, A new model for calculating the effective viscosity of nanofluids, J. Phys. D Appl. Phys. 42 (2009) 055501, 6 pp.

[22] M. Kole, T.K. Dey, Viscosity of alumina nanoparticles dispersed in car engine coolant, Exp. Therm. Fluid Sci. 34 (2010) 677–683.

[23] H.K. Versteeg, W. Malalasekera, An Introduction to Computational Fluid Dynamics, Longman Scientific & Technical, London, 1995, pp. 103–133.

[24] F.W. Dittus, L.M.K. Boelter, Heat Transfer in Automobile Radiators of Tubular Type, University of California Press, Berkeley, CA, 1930, pp. 13–18.

[25] V. Gnielinski, Wärmeübertragung in Rohren, VDI-Wämeatlas, sixth ed., VDI Verlag, Düsseldorf, 2002.

[26] R.S. Vajjha, D.K. Das, P.K. Namburu, Numerical study of fluid dynamic and heat transfer performance of Al_2O_3 and CuO nanofluids in the flat tubes of a radiator, Int. J. Heat Fluid Flow 31 (2010) 613–621.

[27] B.E. Launder, D.B. Spalding, Lectures in Mathematical Models of Turbulence, Academic Press, London, England, 1972.

[28] S. Patankar, Numerical Heat Transfer and Fluid Flow, Taylor & Francis, 1980, pp. 79–135.